Perfect two-dimensional porous alumina photonic crystals with duplex oxide layers

Jinsub Choi, Yun Luo, Ralf B. Wehrspohn,[a] Reinald Hillebrand, Jörg Schilling, and Ulrich Gösele

Max Planck Institute of Microstructure Physics, Weinberg 2, D-06120 Halle, Germany

A perfect two-dimensional porous alumina photonic crystal with 500 nm interpore distance was fabricated on an area of 4 cm^2 via imprint methods and subsequent electrochemical anodization. By comparing measured reflectivity with theory, the refractive indices in the oxide layers were determined. The results indicate that the porous alumina structure is composed of a duplex oxide layer: an inner oxide layer consisting of pure alumina oxide of 50 nm in thickness, and an outer oxide layer of a nonuniform refractive index. We suggest that the nonuniform refractive index of the outer oxide arises from an inhomogeneous distribution of anion species concentrated in the intermediate part of the outer oxide. © *2003 American Institute of Physics.*
[DOI: 10.1063/1.1609033]

I. INTRODUCTION

Periodic dielectric materials allowing to control the flow of light are classified as photonic crystals (PCs).[1] Numerous publications have already been dedicated to realize this concept with various materials. For example, PCs based on silicon are of great interest since they can be easily integrated into the already existing silicon technology.[2,3] Also, opal structures formed by self-assembly have been intensively exploited because of their promising approaches to fabricate three-dimensional PCs.[4]

Due to their low absorption coefficient, excellent thermal stability, and easy handling, porous alumina structures could be potential materials for two-dimensional (2D) PCs in the visible and infrared. The electronic band gap of alumina is 7–9.5 eV. Moreover, it has been suggested that after silver infiltration,[5] porous alumina could be used for metallodielectric photonic crystals associated with an increase in the width of photonic band gaps which may be realized. Metallodielectric photonic crystal could show photonic band gaps for TE mode (*H* polarization) in all directions even though the dielectric constant of the pure alumina in the porous alumina structure is as low as 2.8.[6] In addition, the feasibility of the anodic alumina as a dry etching mask has been introduced to fabricate PCs integrated with semiconductors.[7] For example, this allowed the fabrication of GaAs hole arrays for 2D–PCs.[8] However, since a perfect arrangement of porous alumina channels is required for 2D–PCs, only few studies on porous alumina PCs exist.[9–11] Especially, there are no detailed studies in terms of real porous alumina structures of two layers: an inner layer consisting of a high purity alumina, an outer layer of alumina incorporated with anions, for example, PO_4^{2-}.[12–15]

To fabricate monodomain porous alumina structures, a method to prepattern the surface of aluminum before con-

ventional anodization is a prerequisite. So far, four different methods for prestructuring have been developed: imprint by a dot-like stamp,[16] imprint by a pyramid stamp,[17] electron (e)-beam lithography,[18] and two-step indentation by commercially available gratings.[11] For mass product in the future, imprint methods are considered to be more suitable than e-beam lithography.

In this article, we will discuss in detail large-area PCs based on porous alumina obtained via imprint lithography. The measured reflectivity will be compared with theoretical predictions. Moreover, we will suggest a distribution of anions in the duplex oxide layers of the porous alumina wall to explain the optical properties.

II. EXPERIMENT

A. Imprint

The fabrication procedure of a master stamp is presented in detail elsewhere.[5,17] The master stamp consists of Si_3N_4 pyramids with a height of 260 nm and a lattice constant of 500 nm wafer bonded to a 4 in. silicon substrate. Before indentation, dust on the surface was removed by a strong stream of N_2 gas. Subsequently, the stamp with the size of 1×1 cm^2 was placed on electrochemically polished Al. The pattern on the master stamp was transferred onto the surface of Al under 5 kN/cm^2 with a simple oil press (PW, Paul-Otto Weber GmbH, Germany).

B. Anodization and widening process

The prepatterned aluminum chip was subsequently anodized in 1 wt % phosphoric acid at 195 V for 16 h. The interpore distance of porous alumina is determined by the anodizing potential with a proportionality constant of around 2.5–2.6 nm/V.[12] If the anodization conditions do not match the lattice constant of prepatterns, it is not possible to fabricate the monodomain porous alumina with a high aspect ratio (pore length/pore diameter). The growth rate of pore chan-

---

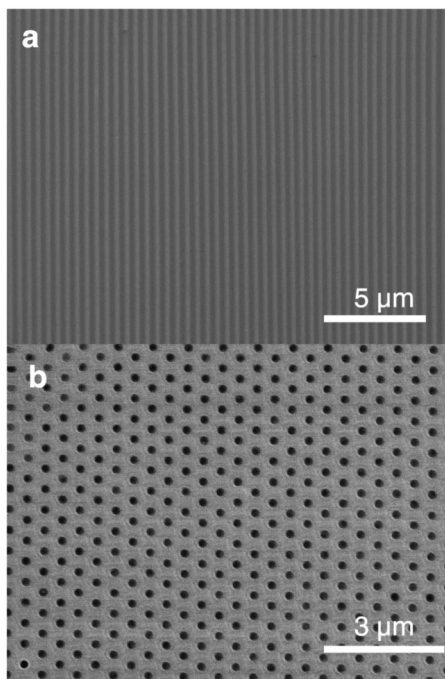[a]Author to whom correspondence should be addressed; electronic mail: wehrspohn@physik.upb.de

FIG. 1. SEM images of porous alumina structure fabricated by the anodization of prepatterned aluminum: (a) Side view and (b) top view.
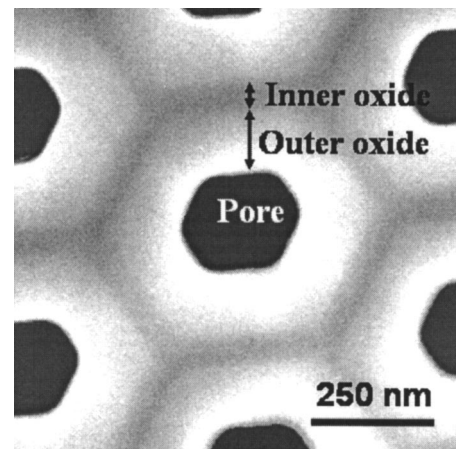

FIG. 2. Transmission electron micrograph (TEM) of porous alumina array obtained by imprint lithography and subsequent anodization (195 V, 1 wt % H_3PO_4). It reveals that the duplex oxide layers consist of inner oxide and outer oxide. Thickness of the inner oxide is 50 nm, whereas that of the outer oxide decreases with increasing the pore diameter (initial diameter: 180 nm) by isotropic etching.

nels in phosphoric acid at 195 V is approximately 5–7 μm/h. The so-obtained porous alumina photonic crystal has an interpore distance of 500 nm and an initial pore diameter of 180 nm. The pore diameter was increased by isotropic chemical etching in 10 wt % phosphoric acid at 30 °C to get different values of r/a (radius/interpore distance) ratio. Typically, the rate of pore widening is approximately 110 nm/h.[5]

C. Optical characterization of the porous alumina

Before optical characterization, porous alumina membranes were prepared by selective etching of aluminum in a $CuCl_2$-containing solution.[12] Afterwards, the membranes were cleaved mechanically and good cleaved planes were confirmed by scanning electron microscopy (SEM). For the optical characterization, the reflectivity of the porous alumina structures with different r/a values was measured along $\Gamma-M$ direction with a Fourier-transform infrared (FTIR) microscope (Bruker, IFS 66) equipped with a UV–CaF_2 beamsplitter, a tungsten lamp, and a HgCdTe detector. The angular aperture of the IR-objective is 30°. A background measurement was performed on a silver mirror as a reference before the actual measurements.

D. Calculations of reflectivity and band structure

Bandstructures of the porous alumina PCs were calculated via the MIT package.[19] In addition, numerical calculations of reflectivity were performed by the transfer-matrix method.[20] The theoretical predictions were compared to the experimental results.

III. DUPLEX STRUCTURE OF POROUS ALUMINA: INNER OXIDE AND OUTER OXIDE

Figure 1 shows the monodomain porous alumina with 500 nm interpore distance and 100 μm length formed under the conditions discussed in experimental section. The structure shows a defect-free array and straight channels, demonstrating that it is suitable to be studied as PCs. In principle, monodomain porous alumina on a cm^2 scale can be fabricated by our imprint method.

Details of porous alumina structure are very similar to those shown by Nielsch *et al.*[12] In Fig. 2, one can see that the inner oxide layer near the cell boundary is about 50 nm thick. The outer oxide layer is between the inner oxide layer and the air pore. In fact, the inner oxide layer is known to be composed of pure alumina oxide, whereas the outer oxide layer has impurities such as incoporated anions.[13] The definition of the inner oxide and the outer oxide in porous alumina is analogous to that in barrier-type alumina where the inner oxide and the outer oxide exist adjacent to aluminum and the electrolyte, respectively.

In this study, it is reasonable to assume that phosphorus (P) and water (H_2O) are major impurities since aqueous H_3PO_4 is used as the electrolyte. Previous studies revealed that in the case of barrier oxide formation in phosphate solution, phosphorus in the form of PO_4^{3-} exists in the outer part and some protons are incorporated in the oxide at the electrolyte/oxide interface.[21]

Moreover, we can see that the duplex layers of inner and outer oxides exist not only in the wall but also in the barrier layer at the pore bottoms (Fig. 3). The thickness of the outer oxide layer in the barrier is exactly the same as that in the wall. However, the inner oxide layer in the center of the hemisphere of the barrier layer is twice as thick as that in the wall, while the inner oxide at the edge of the hemisphere is the same as that in the wall. This observation could be explained by the fact that maximum electric field is concentrated at the pore center.[22]
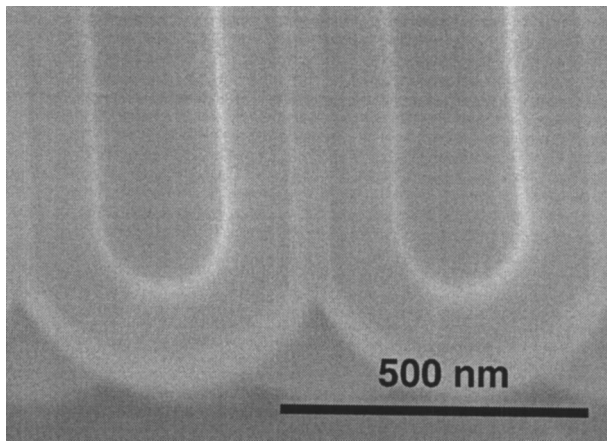
FIG. 3. SEM micrograph of cross section of the porous alumina formed under the same condition of Figs. 1 and 2. The barrier oxide layer, the inner oxide, the outer oxide and the pore are clearly shown. Interpore distance is 500 nm.

IV. OPTICAL CHARACTERIZATION

The reflectivity of the porous alumina structure with different values of the r/a ratio was measured along the $\Gamma-M$ direction by a FTIR equipped with a microscope. The measurement was carried out on a plane cleavage after the alumina structure had been broken carefully. As described in the previous section, the porous alumina structure has duplex oxide layers with different dielectric constants. As a result, the effective dielectric constant of the whole structure is not a constant for different values of r/a ratio. In particular, we will see later that the outer oxide layer has a nonhomogeneous effective dielectric constant depending on the concentration of impurities at different point.

As indicated in Ref. 12, for the lattice constant $a = 500$ nm, the porous alumina structure is only composed of the inner oxide layer when the pore radius $r \geq 200$ nm. Therefore, we first measured the reflectivity of a sample with $r/a = 0.4$ which is composed of only inner oxide. Note that we have taken into account that pores are hexagonal and not round.
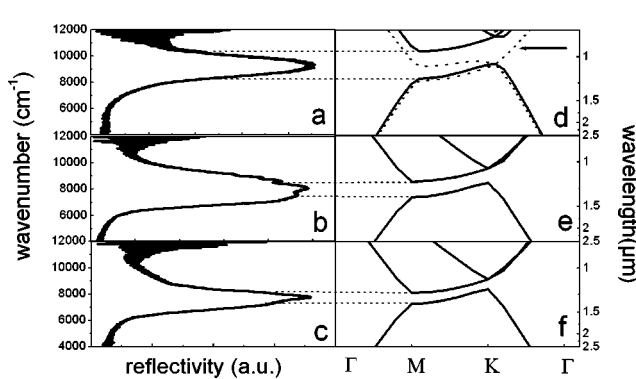

FIG. 4. Comparison of the reflectivity measurements and band structure calculations [$\Gamma-M$ direction, TE (H) polarization] for different values of r/a ratio: (a) $r/a = 0.4$; (b) $r/a = 0.24$; (c) $r/a = 0.18$; (d), (e), and (f) are band structure calculations of (a), (b), and (c), respectively. In picture (d) the band structure also for the TM (E) polarization is shown. The mode marked with an arrow cannot couple to plane waves due to symmetry reasons.

TABLE I. Literature survey of refractive index, n, of alumina. Here, we assume that the dielectric constant of alumina, ϵ, is equivalent to n^2 due to a low absorption coefficient in the visible and infrared ranges.

Ref.	Refractive index	Conditions
23	1.65	Unknown
24	1.67–1.62 @ $\lambda = 0.3$–0.6 μm	3% ammonium tartrate
25	1.64 @ $\lambda = 0.546$ μm	4.25% phosphoric acid (140 V)

Figures 4(a), 4(b), and 4(c) show the reflection spectra in the $\Gamma-M$ direction for the porous alumina with $r/a = 0.4$, 0.24, and 0.18. The stop gaps of TE mode in $\Gamma-M$ direction for these three r/a ratios are 0.96–1.20, 1.17–1.36, and 1.28–1.41 μm, respectively. Because a background spectrum on a silver-coated mirror was taken as a reference before the real measurements, the reflection spectra are in real units. For both polarizations, the dielectric constant of the inner oxide is deduced by the position and width of the maximum reflection (photonic stop gap in $\Gamma-M$ direction) compared to the theoretical calculation for different values of refractive indices. The dielectric constant of the inner oxide, ϵ_{inner}, was determined by the band structure calculation which matches best the measured reflection in the porous alumina with $r/a = 0.4$. Here, ϵ_{inner} is estimated around 2.8 for both E and H polarization, which is in a good agreement with the previously reported dielectric constant of pure aluminum oxide (Table I). Note that among the three dispersion relations [Figs. 4(d), 4(e), and 4(f)] for TE mode, a band gap in all directions is opened for $r/a = 0.40$ and $r/a = 0.24$. Since for the same spectral range, there is no band gap in for the TM polarization, this is not a complete band gap. For example, Fig. 4(d) shows the band structure for both polarizations for $r/a = 0.4$ and $\epsilon_{inner} = 2.8$. The $\Gamma-K$ direction in TM polarization closes the band gap. Please note, that this very band cannot couple to plane waves from outside due to symmetry reasons. This explains why Masuda *et al.*[10] do see a dip in the transmission in this spectral range. The dispersion relation for $r/a = 0.18$ [Fig. 4(f)] does not even open a bandgap for the TE polarization at all but a stop gap in $\Gamma-M$ direction.

In Fig. 5, the measured reflection spectrums of alumina PCs with $r/a = 0.4$ in $\Gamma-M$ direction for both polarizations are compared to calculation by the translight package. For both E and H polarization, the band gap positions observed in the measurement are in good agreement with the calculated ones. In addition, for the TE mode, more than 90% reflectivity within the stop gap is observed, indicating very low losses and high quality structures. For the TM mode, a slight blueshift on the high frequency side implies a stronger angular dependence of the E polarization since the IR objective has an angular aperture of 30°.[26]

After determining the refractive index of the inner oxide, we measured a series of reflectivities of both polarizations for different values of the r/a ratio which represent the different thicknesses of the outer oxide layer. For each polarization, bandstructures were calculated for every value of r/a with a series of dielectric constants of the outer oxide, taking into account that the porous alumina structure has duplex
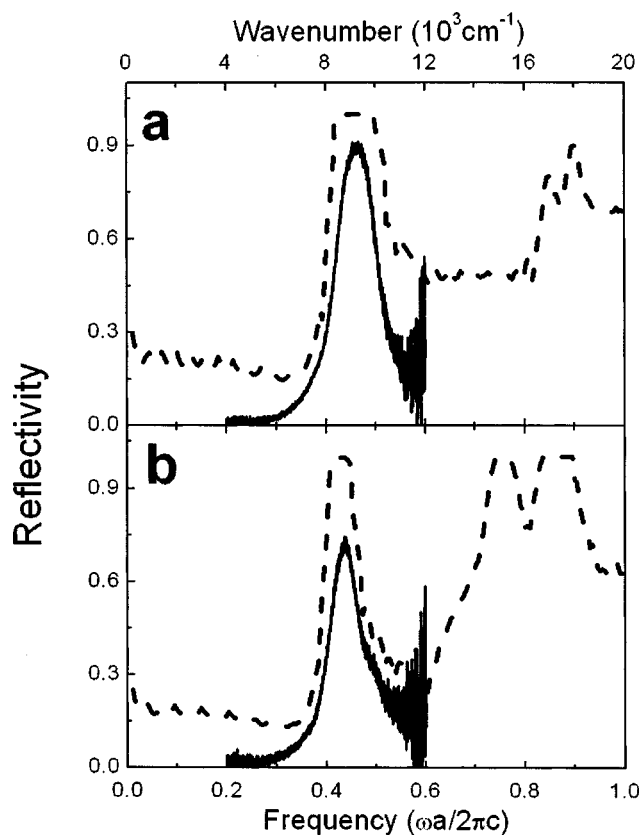
FIG. 5. Reflectivity measured by FTIR microscope (solid lines) and calculation computed by transfer matrix method (dashed lines) in case of r/a $= 0.4$. (a) TE (H) polarization and (b) TM (E) polarization.

FIG. 7. Effective dielectric constant of the outer oxide as a function of the r/a value ($\square$: TE mode and $\bullet$: TM mode). Note that the points where $r/a = 0.4$ represent the dielectric constant of the inner oxide.

oxide layers. As shown in Fig. 6(a), the duplex porous alumina structure is composed of dielectric constants of the air pores ($\epsilon = 1$), the outer oxide layers (non-uniform values of ϵ, e.g., 2.4–2.7), and the inner oxide layers ($\epsilon \simeq 2.8$), which are represented by the black, light gray and dark gray, respectively. The corresponding magnetic field distribution at the M point of the fundamental dielectric band is shown in Fig. 6(b). Note that a mode has the tendency to concentrate most of its displacement energy in the high ϵ area in order to lower its frequency. Since the displacement field is largest along the nodal planes of the magnetic field, the light gray
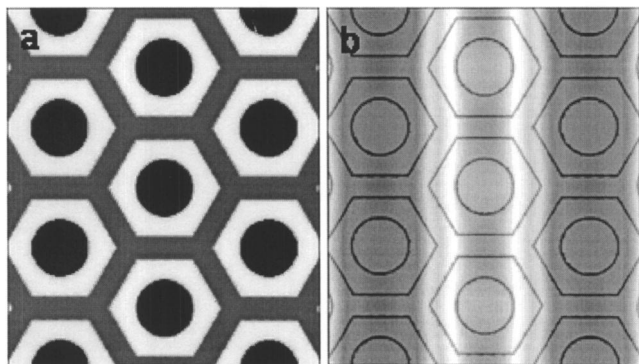

FIG. 6. (a) Map of the dielectric constant for the theoretical calculation in which different values of dielectric constants correspond to different gray scales. The corresponding H-field distribution of the TE mode at the M point of the air band of the fundamental band gap is described in (b).
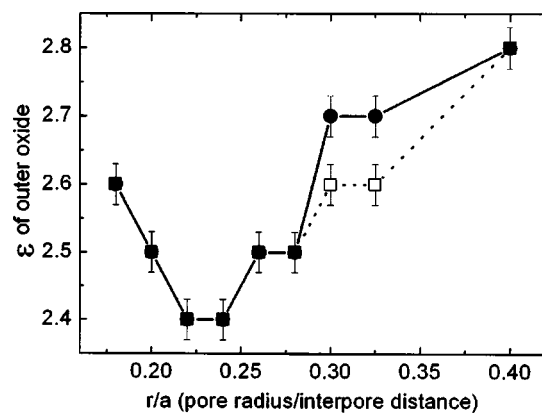
regions are where the displacement energy is concentrated. These regions represent the alumina part, especially the inner oxide layer.

For each polarization, the value of the dielectric constant which gives the best fitting to the measured band structure was selected as the effective refractive index of the outer oxide. This effective dielectric constant in the outer oxide, $\epsilon_{\mathrm{eff,outer}}$, is not a constant for different r/a values. As shown in Fig. 7, for a value of the r/a ratio between 0.18 and 0.33, $\epsilon_{\mathrm{eff,outer}}$ varies from 2.6 to 2.4 and then to 2.6 for the TE mode, from 2.6 to 2.4 and then to 2.7 for the TM mode. Note that when the r/a value is between 0.28 and 0.40, the $\epsilon_{\mathrm{eff,outer}}$ is different for E and H polarization. This reveals the birefringence of the porous alumina structure.

Figure 8 shows the gapmap of the first stop gap positions in $\Gamma - M$ direction calculated by MIT package as well as measured by the FTIR microscope. The agreement between theory and measurement is very good. As the filling factor r/a increases, the band gap edges for both polarizations shift to higher frequency. The band gap widths also increase due to the higher dielectric constrast of the whole structure. In Fig. 8(a), the hatched area shows the calculated photonic band gap frequency range for the TE mode. The maximum gap-midgap ratio is 9.73% for $r/a = 0.40$. The band gap frequencies are higher compared to the results in Ref. 2. This is due to the facts that the real structure of the porous alumina consists of the duplex oxide layers and that the interface between the two oxide layers has a hexagonal shape.

In fact, Masuda *et al.* reported that stopgaps for both polarizations in the porous alumina PCs with $r/a = 0.18$ are observed, which are in a good agreement with theoretical predictions assuming a dielectric constant of 2.8.[10] Note that if we take 2.8 as dielectric constant of the inner oxide and 2.6 as dielectric constant of the outer oxide, the effective dielectric constant of the whole oxide structure is only slightly lower than the value used by Masuda *et al.*

V. DISCUSSION

In this section, the reason for the distribution of the effective dielectric constant in the outer oxide layer will be discussed.
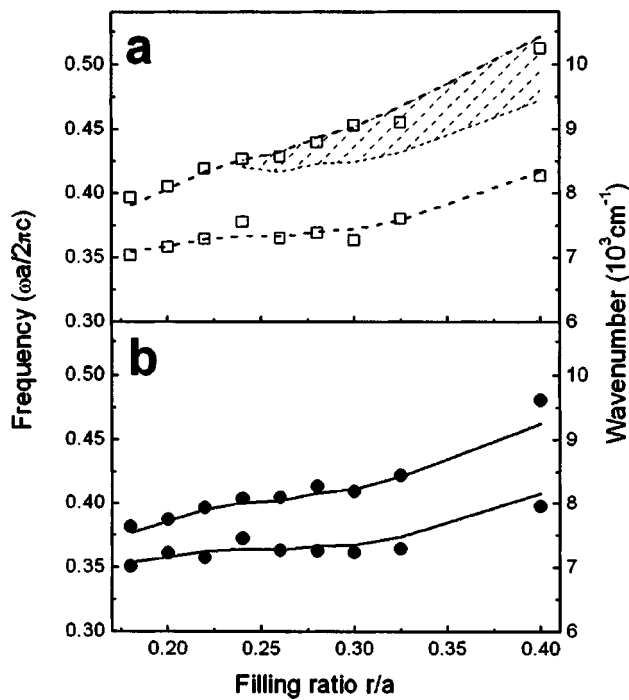
FIG. 8. Map of stop gaps as a function of filling ratio r/a. (a) The TE mode: squares ($\square$) indicate stop gap from the reflectivity measurements in $\Gamma - M$ direction. Dashed lines correspond to theoretical calculations of stop gap. The hatched area indicates calculated photonic band gap in all in-plane directions which is deduced from bandstructure calculations. (b) The TM mode: dots ($\bullet$) represent stop gap from the reflectivity measurements in $\Gamma - M$ direction. The calculated stop gap is shown in solid lines. Note that there is no photonic band gap in all in-plane directions for the TM mode due to the low dielectric constant contrast.
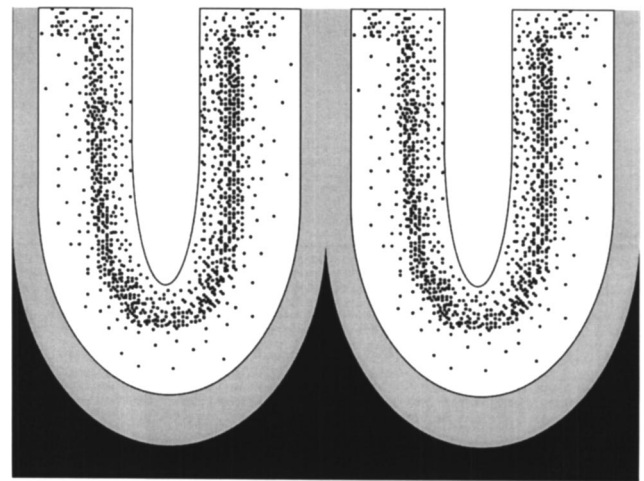

FIG. 9. Schematic diagram of porous alumina oxide layers consisting of inner oxide and outer oxide. Anions (black points) are concentratively distributed in the intermediate part of the outer oxide. Note that the inner oxide in the center of hemispheric scallop of barrier layer is twice as large as that in the edge of hemispheric scallop of barrier layer or in the wall.

The inhomogeneities of the dielectric constant of the whole outer oxide layer might be explained by the nonuniform distribution of anions in the outer oxide layer. Several possible alumina minerals with the different refractive indices should be considered as shown in Table II.

Compared to the dielectric constant of the pure alumina, the anion-incorporated alumina minerals have lower dielectric constants. The more anions are incorporated in the alumina, the lower the dielectric constant. In addition, as the degree of hydrates in the minerals decreases from tri- to mono-, the corresponding refractive index increases. The density of the materials is reduced in a similar way, so that the change in the effective dielectric constant can be attributed to a density modification. For example, for both augelite and wavelite containing phosphorus, the refractive index is similar to or smaller than that in hydrated alumina oxides. It is reasonable to assume that anion complexes containing

phosphorous are concentrated in the intermediate part (Fig. 9). This region corresponds to the minimum dielectric constant in Fig. 7. As the anion contamination decreases towards the inner oxide layer and the outermost oxide layer, the effective dielectric constant for both regions increases. This interpretation is in line with a model for the porous alumina structure suggested by Fukuda and Takahashi *et al.*[27–29] According to their model, the pore wall of porous alumina consists of an inner oxide layer composed of pure alumina and an outer oxide layer. The outer oxide layer again consists of an outermost oxide part and an intermediate oxide part. Takahashi *et al.* claim that the mobility of PO_4^{3-} is responsible for the nonuniform anion concentration.[27,28] Adsorbed anions, for example, PO_4^{3-}, OH^-, and O^{2-}, are pulled into the positively charged electrode by the electric field. Since the size of the phosphorus anion complex is larger than the size of the other anions, the adsorbed PO_4^{3-} migrates more slowly compared with OH^- and O^{2-}. The phosphorus anion complex is delayed in the intermediate part since the attracting force in the intermediate part is weaker than that in electrolyte/outermost oxide interface. As a result, PO_4^{3-} is concentrated in the intermediate part of the outer wall.

VI. CONCLUSIONS

Porous alumina PCs with different values of r/a ratio were fabricated via nanoindentation and subsequent anodiza-

TABLE II. Possible alumina minerals with the different refractive indices (see Ref. 30).

Name	Composition	Refractive index	Density (g/cm^3)
Wavelite	$Al_3(OH)_3(PO_4)_2 \cdot 5H_2O$	$n_\alpha = 1.527$, $n_\beta = 1.535$, $n_\gamma = 1.553$	2.36
Augelite	$Al_2(PO_4)(OH)_3$	$n_\alpha = 1.574$, $n_\beta = 1.576$, $n_\gamma = 1.588$	2.70
Gibbsite or hydrargillite	$\alpha\text{-}Al(OH)_3$	$n_\alpha = 1.57$, $n_\beta = 1.57$, $n_\gamma = 1.59$	2.42
Diaspore	$\beta\text{-}AlO(OH)$	$n_\alpha = 1.694$, $n_\beta = 1.715$, $n_\gamma = 1.741$	3.4
Boehmite	$\alpha\text{-}AlO(OH)$	$n_\alpha = 1.64$, $n_\beta = 1.65$, $n_\gamma = 1.66$	3.44
Corundum	$\alpha\text{-}Al_2O_3$	$n_\alpha = 1.761$, $n_\beta = 1.769$	3.97

tion. The porous alumina structures consist of an inner oxide layer of pure alumina with 50 nm thickness and an outer oxide layer containing impurities such as incoporated anions.

The reflectivity of the porous alumina PCs with the series of r/a ratios (0.18–0.40) was measured and compared with the corresponding bandstructure calculations. Even though complete photonic band gaps are not expected due to the low dielectric constant contrast, photonic stopgaps in both TE and TM polarizations in the $\Gamma-M$ direction are detected in near-infrared regime. In addition, comparison of theory with experiment shows that the outer oxide layer has a nonhomogenous dielectric constant depending on the degree of impurity concentration. For example, the $\epsilon_{\mathrm{eff,outer}}$ varies from 2.6 for $r/a=0.18$, to 2.4 for $r/a=0.22$, and to 2.7 for $r/a=0.33$ for TM mode. It can be concluded that the outer oxide layer consists again of an outermost part and an intermediate part. It is suggested that the phosphorous anion complex incorporated in the outer oxide layer is concentrated in the intermediate part of the outer oxide layer.

ACKNOWLEDGMENTS

[1] J. D. Joannopoulos, R. D. Meade, and J. N. Winn, *Photonic Crystals* (Princeton University Press, Princeton, NJ, 1995).
[2] R. B. Wehrspohn and J. Schilling, MRS Bull. **26**, 623 (2001).
[3] A. Birner, R. B. Wehrspohn, U. Gösele, and K. Busch, Adv. Mater. (Weinheim, Ger.) **13**, 377 (2001).
[4] Y. N. Xia, B. Gates, Y. D. Yin, and Y. Lu, Adv. Mater. (Weinheim, Ger.) **12**, 693 (2000).
[5] J. Choi, G. Sauer, K. Nielsch, R. B. Wehrspohn, and U. Gösele, Chem. Mater. **15**, 776 (2003).
[6] H. van der Lem and A. Moroz, J. Opt. A, Pure Appl. Opt. **2**, 395 (2000).
[7] H. Masuda, K. Yasui, M. Watanabe, K. Nishio, M. Nakao, T. Tamamura, T. N. Rao, and A. Fujishima, Electrochem. Solid-State Lett. **4**, G101 (2001).
[8] M. Nakao, S. Oku, H. Tanaka, Y. Shibata, A. Yokoo, T. Tamamura, and H. Masuda, Opt. Quantum Electron. **34**, 183 (2002).
[9] H. Masuda, M. Ohya, H. Asoh, M. Nakao, M. Nohtomi, and T. Tamamura, Jpn. J. Appl. Phys., Part 2 **38**, L1403 (1999).
[10] H. Masuda, M. Ohya, K. Nishio, H. Asoh, M. Nakao, M. Nohtomi, A. Yokoo, and T. Tamamura, Jpn. J. Appl. Phys., Part 2 **39**, L1039 (2000).
[11] I. Mikulskas, S. Juodkazis, R. Tomašiunas, and J. G. Dumas, Adv. Mater. (Weinheim, Ger.) **13**, 1574 (2001).
[12] K. Nielsch, J. Choi, K. Schwirn, R. B. Wehrspohn, and U. Gösele, Nano Lett. **2**, 677 (2002).
[13] G. E. Thompson and G. C. Wood, Nature (London) **290**, 230 (1981).
[14] F. Keller, M. S. Hunter, and D. L. Robinson, J. Electrochem. Soc. **100**, 411 (1953).
[15] J. P. O'Sullivan, G. C. Wood, Proc. R. Soc. London, Ser. A **317**, 511 (1970).
[16] H. Masuda, H. Yamada, M. Satoh, H. Asoh, M. Nakao, and T. Tamamura, Appl. Phys. Lett. **71**, 2770 (1997).
[17] J. Choi, K. Nielsch, M. Reiche, R. B. Wehrspohn, and U. Gösele, J. Vac. Sci. Technol. B **21**, 763 (2003).
[18] A.-P. Li, F. Müller, and U. Gösele, Electrochem. Solid-State Lett. **3**, 131 (2000).
[19] The MIT photonic-bands (MPB) package, S. G. Johnson, MIT (http://ab-initio.mit.edu/mpb/).
[20] Translight package, A. L. Reynolds, University of Glasgow (http://userweb.elec.gla.ac.uk/a/areynolds/).
[21] H. Takahashi, K. Fujimoto, H. Konno, and M. Nagayama, J. Electrochem. Soc. **131**, 1856 (1984).
[22] V. P. Parkhutik and V. I. Shershulsky, J. Phys. D **25**, 1258 (1992).
[23] K. Huber, J. Colloid Sci. **3**, 197 (1948).
[24] G. Hass, J. Opt. Soc. Am. **39**, 532 (1949).
[25] S. Nakamura, M. Saito, L.-F. Huang, M. Miyagi, and K. Wada, Jpn. J. Appl. Phys., Part 1 **31**, 3589 (1992).
[26] R. Hillebrand and R. B. Wehrspohn (unpublished).
[27] Y. Fukuda, Nippon Kagaku Kaishi 1868 (1974): [Trans. Nat. Res. Inst. Metals **17**, 25 (1975)].
[28] H. Takahashi and M. Nagayama, Nippon Kagaku Kaishi 453 (1974).
[29] S. Ono, H. Ichinose, and N. Masuko, Corros. Sci. **33**, 841 (1992).
[30] *CRC Handbook of Chemistry and Physics*, 76th ed., edited by D. R. Lide (CRC Press, New York, 1995), pp. 4–132.